American Journal of Engineering and Applied Sciences

Original Research Paper

Thermo Optical Properties and Related Electronic Polarizabilities of MoO_3 Thin Films Using Ellipsometry

Zahid Hussain

Imperial College of Science, Technology and Medicine, Department of Electrical and Electronics, Engineering Exhibition Road, London SW7 2BT UK

Article history
Received: 20-01-2019
Revised: 18-02-2019
Accepted: 01-04-2019

Corresponding Author:
Zahid Hussain
Imperial College of Science, Technology and Medicine
Department of Electrical and Electronics Engineering
Exhibition Road, London SW7 2BT UK
Email: (hzzhussain@aol.com)

Abstract: Thermo optical properties are reported for thermally evaporated MoO_3 thin films using ellipsometry. The values of TOCs: dn/dT and dk/dT relating to MoO_3 thin films are found to be negative and positive, respectively over the temperature range 295-460 K and also are found to have the same trend over the range 120-300 K, and have values of the order of 10^{-4} K^{-1} and 10^{-5} K^{-1}, respectively in the visible part of spectral range. The values of electronic polarizability were determined to be in the range from 8.2 to 8.21×10^{-24} cm^3 in the temperature range 120-460 K and over the same part of spectral range. Vacuum-heating and annealing in an oxygen plasma environment certainly assists in reducing a large amount of porosity in the films, but these series of actions yield irreversible changes in the morphology of the films. Once the films during oxidative-annealing turned into black in colour and new reduced chemical states were produced, then after that, original states of the films were very hard to restore. Ellipsometric data of MoO_3 thin films at or above the room temperature in the range 295-460 K seems to be controlled by first-order kinetics and could be interpreted in terms of polaronic excitations and hoppings. During the in-situ cooling runs, the changes in the ellipsometric data are interpreted in terms of bipolaronic excitations, but the possibility of simultaneous presence of polaronic and bipolaronic states cannot be ignored over the investigated temperature range.

Keywords: Optoelectronics, Electro-Optical Devices, Electro-Optical Materials, Optical Materials, Optical Properties, Opto-Electronic Properties, Electrochromic Properties, Optical Constants, Ellipsometry, Thin Films

Introduction

Transition metal oxides (WO_3 or MoO_3) are electrochromic materials, which have relatively large applications in display devices and smart optical windows (Gesheva *et al*., 2012; Hsu *et al*., 2008; Scrosati, 1990; Granqvist, 2014). MoO_3 has been extensively used in image recording and in stable thin holograms (Tubbs, 1974; Anwar and Hogarth, 1988). MoO_3 has been widely used in various organic-based electronic devices, including Organic Light Emitting Devices (OLEDs) (Matsushina *et al*., 2007; You *et al*., 2007; Haitao and Xiang, 2013), Organic Thin Film Transistors (OTFTs) (Chu *et al*., 2005; Kumaki *et al*., 2008), organic photovoltaic cells (Shrotriya *et al*., 2006; Tseng *et al*., 2012) and Organic Solar Cells (OSCs) (Zhang *et al*., 2010; Hori *et al*., 2009). MoO_3 finds application as a cathode material in the development of high-energy density solid state microbatteries (Rao *et al*., 2013; Cheng *et al*., 2006). Molybdenum oxide films and nano-crystals also find applications in catalysis (Manivel *et al*., 2015; Chen *et al*., 2010), ethonal and gas sensing (Bai *et al*., 2015; Khojier *et al*., 2014; Touihri *et al*., 2017) and in lubricants (Prasad *et al*., 2003; Hosono *et al*., 2005; Wang *et al*., 1999).

Molybdenum trioxide is a transparent, partly ionic 4d transition metal oxide. The study of the crystal structure of the molybdenum oxide was done by several workers and it was found to be a shear structure consisting of large slabs, joined along the crystallographic shear

planes (Bertrand *et al*., 1985; Punitha *et al*., 2014). MoO_3 can be easily prepared either in single crystal or in thin layer form and can display both electronic and ionic conductivity (Schollhorn *et al*., 1976; Li *et al*., 2016). When prepared in thin film form at room temperature, it has been declared to be sub-stoichiometric MoO_{3-y}, where y is a small fraction (Wang *et al*., 2012; Madhavi *et al*., 2013). Thermally evaporated oxygen deficient molybdenum trioxide thin film has been revealed to be n-type semiconductor and has band gap in the range 2.9–3.15 eV (Svensson *et al*., 1988; Hussain, 2001; 2002a). Moreover, in these thin films, Mo-Mo distances are too large to form the metallic bonds probably due to lack of overlap of 4d-wave functions (Colaitis, 1991; Sian *et al*., 2004).

After publishing ellipsometric data on M_xWO_3 (M = H^+, Li^+, Na^+) and A_xMoO_3 (A = H^+, Li^+) bronzes (Hussain, 2018a; 2018b) and before publishing temperature dependent ellipsometric data on tungsten and molybdenum bronzes, our present focus is entirely on to explore the optical constants of MoO_3 thin films using ellipsometry.

Investigations on the preparation and optical constants of sub-stoichiometric MoO_3 thin films are quite essential for their effective use in microbatteries, electrochromic and microelectronic devices. It should be noted that we have already published temperature dependent ellipsometric data on WO_3 thin films (Hussain, 1999).

There is a plethora of structural analysis in the literature that MoO_3 thin films still remain microcrystalline when heated below 623 K whereas films heated above 623 K turn into crystalline phase (McEvoy and Stevenson, 2003; Sian *et al*., 2004; Szekeres *et al*., 2002). It has also been concluded that amorphous or microcrystalline phase shows superior intercalation capability to crystalline phase (Sian *et al*., 2004; Szekeres *et al*., 2002). We have also observed the better electrochromic performance for the "as deposited room temperature prepared films" and also for the heat treated films in the visible spectral region and over the temperature range 295-460 K.

In this paper, we report temperature dependent ellipsometric measurements on MoO_3 thin films prepared on unheated substrate by thermal evaporation. High precision single wavelength manual ellipsometry was used at fixed angle to measure in situ temperature dependent optical constants of MoO_3 thin layers. We have also measured mass densities of MoO_3 thin films in the temperature range 100-460 K. Thermo optic coefficients and electronic polarizabilities are also calculated in the visible spectral region and over the same temperature range.

The reported data has also been interpreted using polaronic and bipolaronic excitations and transitions regarding structural transformations during heating and cooling treatments.

Ellipsometry

Ellipsometry is an optical technique that measures changes in polarization (phase, Δ and amplitude, Ψ) of monochromatic light reflecting from matter and these standard ellipsometric parameters Ψ and Δ are related to the complex ratio of reflection coefficient for light polarized parallel *p* and perpendicular *s* to the plane of incidence. The mathematical expression (Azzam and Bashara, 1977; Tiwald, 2016) for this ratio is:

$$\rho = \frac{r_p}{r_s} \tan \Psi e^{i\Delta}, \tag{1}$$

Where:

$$\tan \psi = \frac{|r_p|}{|r_s|}, \tag{2}$$

and:

$$\Delta = \delta_p - \delta_{s*} \tag{3}$$

The value of tan Ψ gives the differential change in amplitude and Δ measures differential phase change. δ_p and δ_s are the phase factors of the complex Fresnel pseudo-reflection coefficients r_p and r_s, respectively.

High precision single wavelength manual ellipsometry at fixed angle was choosen for in situ heating and cooling experiments in order to generate a series of data on the optical constants of MoO_3 thin films in the visible range of solar spectrum. The related microstructural changes in the films were also monitored using temperature dependent mass density data.

Thickness of each film was measured by an independent technique, Talysurf and its value was compared directly with the auto-ellipsometer and with the ellipsometric numerical model while choosing the real part of the thickness with minimum imaginary number. Once the ellipsometric measurements of Δ and Ψ are determined and the thickness is properly evaluated, the other unknown parameters, real part of the refractive index (n) and index of absorption (k), can in principle be calculated using suitable computer program.

Experimental

Preparation of MoO_3 Thin Films

The source material (Koch light Ltd) was prepared by taking molybdenum powder and heaing in a platinum

crucible in air at a temperature~673 K for 20 h and then for 12 h at 973 K. This caused heavy sintering and grain growth and ultimately the obtained material (of purity 99.9%) was white in colour. Examination of the mass under the optical microscope revealed crystallites of typically 80 μm in diameter. The sintered material was broken into small lumps and put into strips, prior to evaporation. The vacuum chamber base pressure was about 1×10^{-6} mm Hg; and there was a liquid nitrogen cold trap in the chamber, whose function was to reduce the water vapour pressure. The vacuum chamber was equiped with a stainless steel shutter, which was used to block the substrates (7059 glass slide and I.T.O glass plate) from the Mo boat during outgassing. With the shutter in closed position, MoO_3 powder was outgassed at 823 K for 30 min and then heated to 1023 K for 8 min for more dehydration. The current (the temperature) was then increased in order to bring the powder to its melting point. When the temperature was further raised to 1123 K, liquid nitrogen was used to decrease the base pressure to ~ 5×10^{-7} mm Hg. At this stage, the shutter (blocking the substrates) was opened and the films of thicknesses between 0.25 μm and 0.45 μm were attained with a deposition rate of about 12-14 Å/sec. Film deposition rate was constantly monitored with a quartz crystal oscillator at a boat-to-substrate distance of 20 cm. Talysurf measurements (average of four measurements) for the film thicknesses were accurate to a maximum precision of ±30Å.

Freshly evaporated MoO_3 thin films were slightly blue, perhaps due to oxygen deficiency, or because of water or hydroxyl groups present in MoO_3. Difference in the substrate temperature and variation in evaporation rate will give rise to films of different concentration of oxygen vacancies. The reported evaporated thin films are a highly disordered micro-crystalline in structure with grain size of about 60Å, as estimated by our **TEM** and **X-rays** studies (Hussain, 2007; Evans, 1987). The micro-characteristics of the reported films have also been confirmed by other workers (Shiojiri *et al*., 1979; Julien *et al*., 1995).

Calibration and Operation of Manual Ellipsometer

All the optical components of manual ellipsometer were aligned according to some standard procedure. Full details of the alignment and calibrations are described elsewhere (Hussain, 1999; Azzam and Bashara, 1977).

A schematic of the whole apparatus is shown in Fig. 1 Red light (He-Ne laser) was passed through the polarizing section of the instrument (PSG): Consisting of a linear polarizer (P) and a quarter wave plate, Q (or a Compensator, C). This section is called the polarization state generator. After transmitting through the polarizing section of the instrument, the beam struck the sample cell at an angle ~ 60° and changed into elliptically polarized light. This state of polarization was monitored by the rotational azimuth positions of the polarizer and quarter wave plate. Vacuum cryostat was built up with the ability to heat and cool the samples over a broad range of temperature, i.e., 100<T<400 K. The sample cell temperature was monitored through alumel-cromel thermocouple and regulated by a controller. After reflecting by a sample, the modified state of polarization was then controlled by the analyzing section of the instrument (PSD). This section is called the polarization state detector. It consisted of a linear analyzer (A) followed by a narrow pass filter. And then it is followed by a photomultiplier tube connected to Keithly for monitoring the output signal. At extinction, the polarizer azimuth, P, gave a measure of Δ; and the analyzer azimuth, A, delivered a value of Ψ. After alignment, the maximum uncertainty in Δ and Ψ in an open air were found about ±0.02° and ±0.01°, respectively and with an in situ manual ellipsometer fitted with fused quartz inlet and exit optical windows, the maximum calibration errors in Δ and Ψ were about ±0.05° and ±0.02°, respectively. Nevertheless, four-zone ellipsometric measurements were always made in order to minimize systematic errors.

Experimental Results and Error Analysis

The relations of (Ψ and Δ) to (P and A) in four zones at extinction settings are given by equations (Azzam and Bashara, 1977; Tiwald, 2016):

$$A_i = a_p (or\ a_s) = \pm\psi_i \quad (4)$$

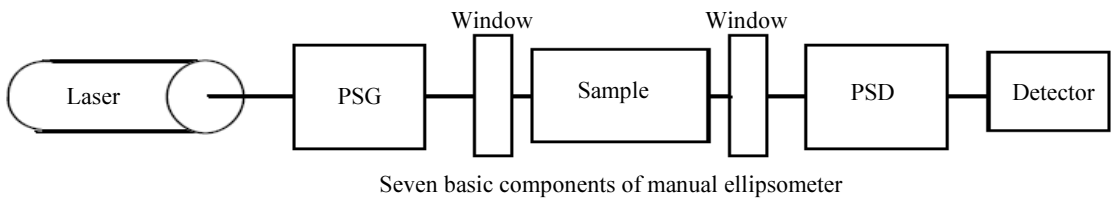

Fig. 1: Schematic for seven basic components of the manual ellipsometer

And:

$$2p_i \pm \pi/2 = \pm(-1)^i \Delta_i, \quad (5)$$

where, i = 1, 2, 3, 4. And a_p or a_s (depending upon zone) denotes the analyser azimuth angle and p is the polarizer azimuth angle. The quantities to be determined from the experimental data (Δ, ψ) using ellipsometric equations are the thickness of the film (t_f), the real part of the refractive index (n) and the extinction coefficient (k).

Ellipsometric Eq. (1) was solved by converting McCrackin package (McCrackin, 1969) into Fortran 77 version and also some modifications were made according to the experimental situation. We determined thickness of each film (t_f) from an independent technique, talysurf and after inserting the values of thickness (t_f) into the fortran program, (n, k) values of different samples of MoO_3 thin films under different temperature conditions were computed directly from the experimental data (Δ and Ψ).

A comparison between manual and auto ellipsometric data is shown in Table 1, which indicates that the manual ellipsometric components were aligned to very high precision. The experimental data (Δ and Ψ) and the related results under different temperature conditions are printed in Tables 2-4 and the respective plots (along with error bars) Vs temperature are displayed in Figs. 2-4. Vacuum-annealed and oxidative-annealing data are also printed in Tables 5 and 6 and their respective plots Vs time are shown in Figs. 5 and 6. A plot of (n, k) of MoO_3 thin film Vs substrate temperature is also shown in Fig. 7.

For a clean surface (7059 glass), a change of ±0.02° in the measurement of the angle of incidence due to optical window strain gives a net change of ±0.02° in Ψ value, which gives an error in n of about δn = ±0.00071.

Table 1: Manual and Auto ellipsometric (comparative) data on MoO_3 thin film (taken at room temperature)

	ϕ~60° λ = 632.8 nm				
Type	Thickness (μm)	Δ (°)	Ψ (°)	n	k
Manual	0.295	124.62	10.16	2.1222	0.00987
Auto	0.298	118.32	10.44	2.1161	0.01012
Manual	0.303	104.91	9.26	2.1272	0.00190
Auto	0.305	106.80	9.52	2.1220	0.00210

Table 2: Vacuum-ellipsometric reversibility (check) data on the evaporated MoO_3 thin film in the temperature range 295 K≤T≤373 K

	Thickness = 0.30 μm ϕ=60.32°			
Temperature (K)	Δ (°)	Ψ (°)	n	k
Heating cycle				
295.0	109.94	9.35	2.1255	0.00440
333.0	115.66	9.59	2.1052	0.00518
373.0	125.21	10.05	2.0642	0.00332
Cooling cycle				
333.0	133.60	10.39	2.0251	0.0019
297.0	131.23	10.50	2.0365	0.00263

Table 3: Vacuum-ellipsometric temperature dependent data on MoO_3 thin film

	Thickness = 0.288 μm ϕ = 60.33°			
Temperature (K)	Δ (°)	Ψ (°)	n	k
Heating cycle				
295.0	131.20	11.73	2.12734	0.00580
373.0	136.75	11.66	2.09824	0.00390
413.0	144.36	11.49	2.05586	0.00370
453.0	149.77	11.60	2.02871	0.00595
Cooling cycle				
373.0	148.88	11.44	2.03184	
	0.00322333.0	149.02	11.41	2.02949
	0.00185295.0	148.25	11.40	2.03330
	0.00107			

Table 4: Vacuum-low-temperature ellipsometric measurements on MoO_3 thin film using liquid nitrogen as a coolant and directing the temperature with a 407 controller

	Thickness = 0.322 μm ϕ = 60.32°			
Temperature (K)	Δ (°)	Ψ (°)	n	k
First cooling cycle				
297.0	27.49	10.53	2.1240	0.01592
229.0	-31.89	9.18	2.1777	0.00996
217.0	-31.42	9.04	2.1773	0.00967
209.0	-32.67	9.08	2.1784	0.00965
175.0	-48.09	4.91	2.1828	0.00508
Second cooling cycle				
241.0	-42.49	4.73	2.1786	0.00511
145.0	-52.91	4.47	2.1844	0.00742
129.0	-43.79	7.08	2.1852	0.00283
Third cooling cycle				
249.0	-45.51	4.02	2.1780	0.00821
195.0	-37.48	7.74	2.1809	0.00559
157.0	-48.22	5.10	2.1835	0.00440
Back to room temperature				
298.0	40.03	2.65	2.1296	0.01602

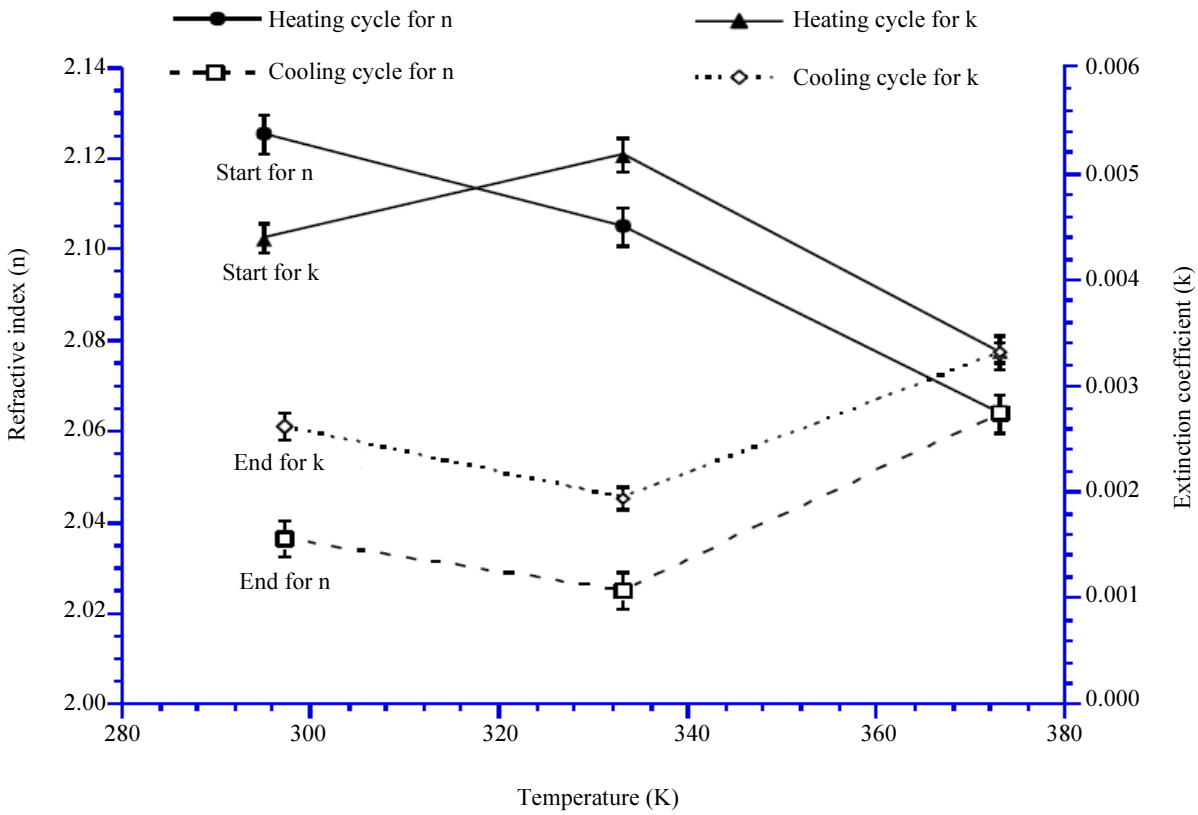

Fig. 2: Plot of the optical constants (n, k) Vs temperature, of MoO_3 thin film in the range 295-373 K

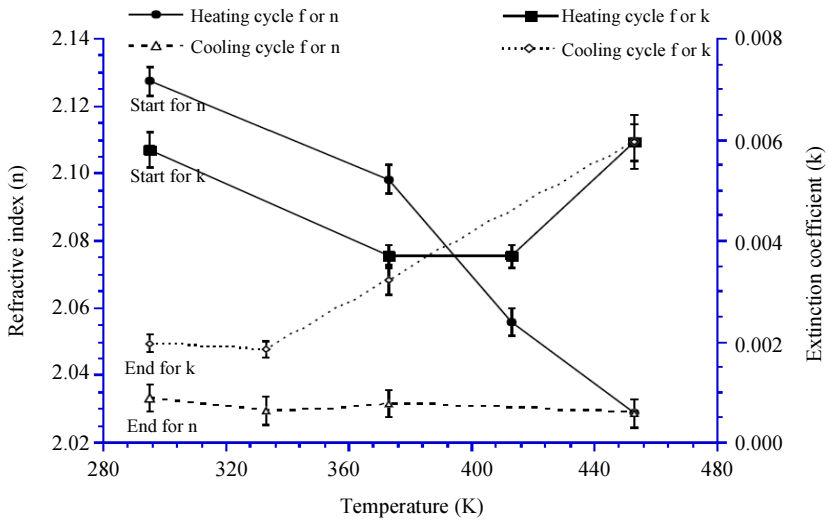

Fig. 3: Plot of optical constants (n, k) Vs temperature, of MoO_3 thin film in the range 295-460 K

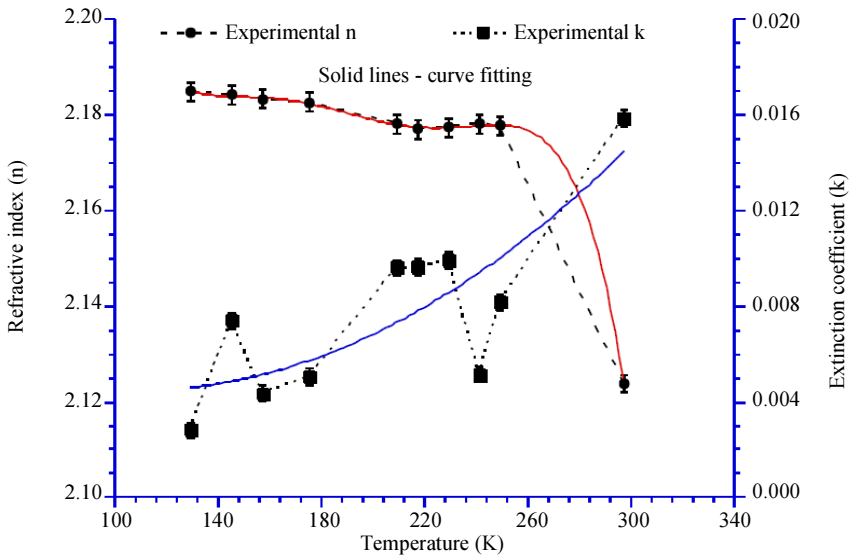

Fig. 4: Plot of optical constants, (n, k) Vs temperature, of MoO_3 thin films in the range 120-300 K

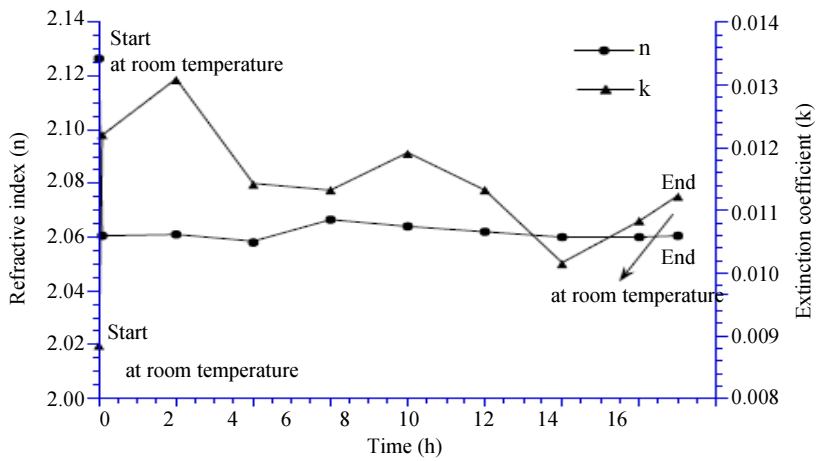

Fig. 5: Plot of optical constants, (n, k) Vs time, of MoO_3 thin film being annealed at temperature T = (413±1) K

Table 5: Vacuum-annealed ellipsometric data on evaporated MoO_3 thin film upheld at a temperature, T = 413 K for different periods of time

	Thickness = 0.42 μm ϕ = 60.33°				
Temperature (K)	Time (h)	Δ (°)	Ψ (°)	n	k
Heating cycle					
295.0		122.54	9.86	2.1268	0.00886
413.0		-87.93	4.09	2.0608	0.01221
413.0	2.0	-90.22	3.96	2.0611	0.01219
413.0	2.0	-83.51	4.05	2.0586	0.01143
413.0	2.0	-92.48	4.67	2.0667	0.01133
413.0	2.0	-90.91	4.39	2.0642	0.01192
413.0	2.0	-87.47	4.36	2.0623	0.01133
413.0	2.0	-82.72	4.43	2.0603	0.01016
413.0	2.0	-84.09	4.27	2.0601	0.01080
Cooling cycle (back to room temperature)					
297.0	1.0	-85.80	4.25	2.0608	0.01123

Table 6: Vacuum-annealed and oxygen plasma treated ellipsometric data on MoO_3 thin film upheld at a temperature, T = 453 K and with a pressure of the order of 10^{-2} torr

	Thickness = 0.40 μm ϕ = 60.33°					
Type	Time (h)	Temperature (K)	Δ (°)	Ψ (°)	n	k
Heating cycle						
		298.0	123.94	10.12	2.1221	0.00887
		453.0	-91.85	4.89	2.0677	0.01045
Annealing	4.0	453.0	-176.38	6.48	1.9848	0.05186
	1.0	453.0	-176.49	6.48	1.9848	0.05186
	6.0	453.0	-160.04	5.04	2.1090	0.05391
Oxygen	1.0	453.0	-158.76	4.53	2.0984	0.05274
Plama	2.0	453.0	-157.83	4.77	2.1036	0.05196
Annealing	4.0	453.0	-162.62	4.23	2.0910	0.05557
	10.0	453.0	-174.44	2.99	2.0585	0.05889
	8.0	453.0	143.15	3.28	2.0079	0.07989
Cooling cycle (back to room temperature)						
	1.0	297.0	142.20	3.27	2.0059	0.07979
Auto ellipsometer		**297.0**	**127.08**	**3.52**	**1.9729**	**0.08399**

*In the absence of plasma, the pressure is of the order of 10^{-5} torr

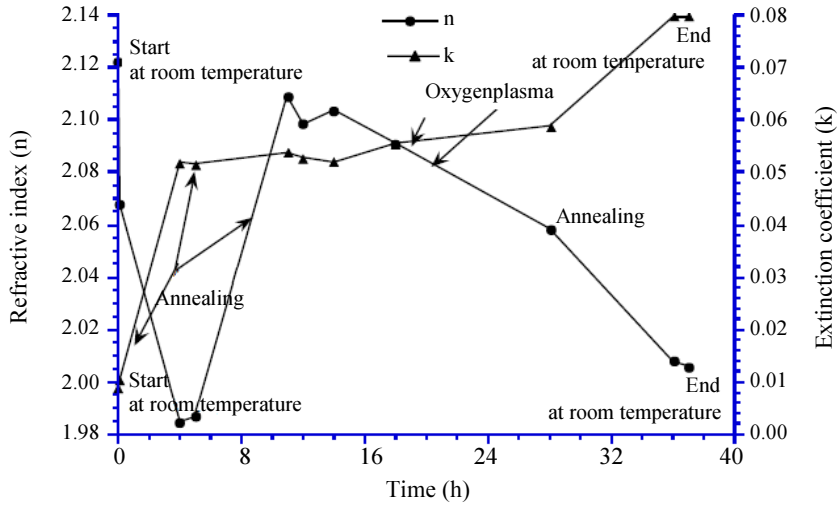

Fig. 6: Plot of optical constants (n, k) Vs time, of MoO_3 thin film being annealed at temperature T = (453±1) K under an oxygen plasma atmosphere

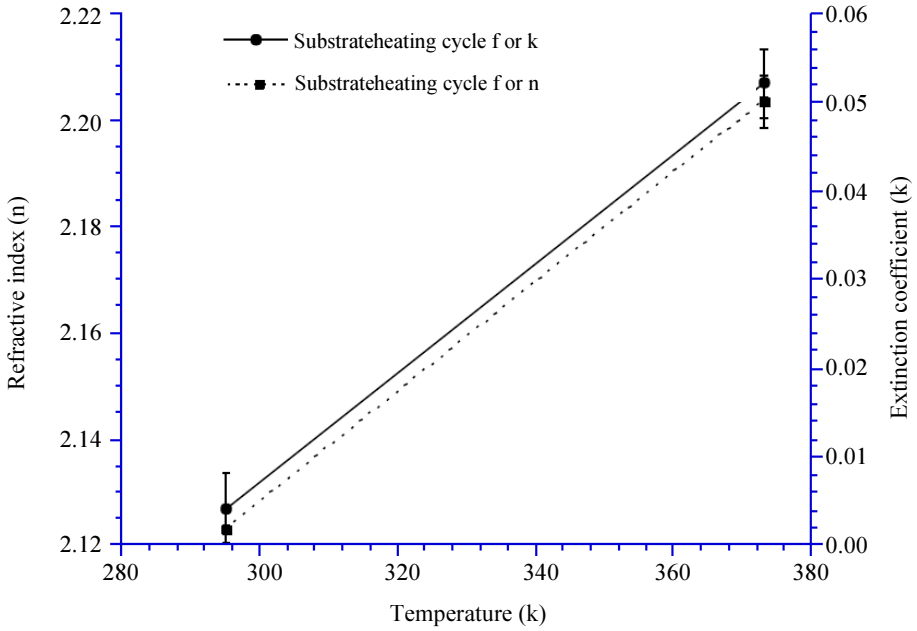

Fig. 7: Plot of optical constants (n, k) of MoO_3 thin film Vs substrate temperature

Similarly, a change of ±0.04° in Δ due to same degree of strain brings a net change in the index of absorption of about δk = ±0.0005. Additionally, an uncertainity of ±30Å in the thickness measurements when added to the above errors, gives a total error in n of about Δn = ±0.0031 and a total error in k of about Δk = ±0.002 for a film covered 7059 glass.

Ellipsometric temperature dependent data for a MoO_3 thin film over the temperature range 100<T<460 K gives an extra uncertainity in n of about Δn′ = ±0.0019 and in k of about Δk′ = ±0.003. Uncertainties due to oxygen plasma or because of different annealing conditions have not been taken into account in the error analysis.

Discussion

Structure and Temperature Dependent Phase Transitions

Molybdenum oxide has one stable orthorhombic symmetry (space group B6nm) (Tubbs, 1974), i.e., α–MoO_3 which is white; and the other two metastable polymorphs, β–MoO_3 and β′–MoO_3 which have framework structures similar to ReO_3 (Itoh *et al*., 2001; Parise *et al*., 1987). Due to stronger distortion of the metal-oxygen octahedra in the molybdenum than in the tungsten, the structure of α–MoO_3 is not like ReO_3 (Itoh *et al*., 2001; Baker and Dickens, 1989). In the α-orthorhombic phase it exhibits two-dimensional layered structure, as shown in Fig. 8(a), with a = 3.96Å, b = 13.86Å and c = 3.69Å (Dickens *et al*., 1979; Scanlon *et al*., 2010; Diaz *et al*., 2010). It consists of zigzag chains of MoO_6 octahedra linked through vertices and has fragile Van der Waals forces in between the layeres. Also in this structure, all oxygen ions are not equivalent and therefore Mo-O distance varies from 1.67 to 2.34Å (Baker and Dickens, 1989; Scanlon *et al*., 2010; Kuzmin and Purans, 1993), as shown in Fig. 8(b). Freshly prepared β–MoO_3 is to have a yellow colouration similar to WO_3 (Baker and Dickens, 1989; Carcia *et al*., 1987) and certain aspects of the stereochemistry observed for β′–MoO_3 are also common in β–MoO_3 (Parise *et al*., 1987; Baker and Dickens, 1989). β–MoO_3 can be converted into white α-phase (α–MoO_3. H_2O or α–MoO_3) by topotactic transformation when heated above 623 K (Parise *et al*., 1987; Baker and Dickens, 1989), where white α–$MoO_3.H_2O$ has a structure closely related to that of α–MoO_3, (Baker and Dickens, 1989; Gunter, 1972), consisting of two fold chains of edge-sharing MoO_6 octahedra with co-ordinated water molecules attached to molybdenum atoms. β′–MoO_3 as sketched in Fig. 9(a) has MoO_6 octahedra linked by sharing corners and is found to be isostructural with the monoclinic form of WO_3. Mo-O bond lengths (Itoh *et al*., 2001; Parise *et al*., 1987) in this structure are shown in Fig. 9(b). β′–MoO_3 may be considered as an intermediary structural state between perovskite and the modified layered form of MoO_3.

The molybdenum trioxide films formed at higher substrate temperature normally emerge as polycrystalline with α–β mixed phase. On thermal treatment in air at about 653 K for 4 h, the films are transformed to the

α−phase (Wang *et al*., 2012; Scanlon *et al*., 2010). The transformation from α+β mixed phase to α−phase was also observed in the films deposited at 523 K (Wang *et al*., 2012; Sabhapathi *et al*., 1995). Side views of corner and edge sharing MoO_6 octahedra of β−MoO_3, α−MoO_3 and α−MoO_3. H_2O along the [100] plane are shown in Figs. 10(a) and (b).

Crystalline WO_3 and V2O_5 were found to have stable crystallographic structure, even on heating in UHV up to 850 K (Kihlborgn and Magneli, 1955) and 823 K (Bursill, 1969), respectively; but MoO_3 loses its stoichiometry and starts to decompose on heating above 773 K under vacuum (Rao *et al*., 2013; Diaz *et al*., 2010; Ohfuji, 1984). Diffusion of oxygen through the MoO_3 lattice becomes rapid at higher temperature and this temperature allows the formation of adsorption and reaction sites for the molecular state of oxygen. In the case of MoO_3 thin films, prepared (on cold substrates) either by evaporation or by sputtering techniques, the information relating to their structures is scanty and in the literature such films are declared as amorphous (Tubbs, 1974; Rao *et al*., 2013; Shiojiri *et al*., 1979; Carcia *et al*., 1987). A series of lower oxides, known as $MoO_{2.95}$, $MoO_{2.89}$, $MoO_{2.88}$, $MoO_{2.85}$, $MoO_{2.75}$ lie in between MoO_3 and MoO_2 (Hansen and Andersson, 1988; Kumada *et al*., 1986; Kihlborg, 1959). On heating around 800K, MoO_3 thin film (Epifani *et al*., 2004; So *et al*., 1988) or single crystal (Hansen *et al*., 1988; Wold *et al*., 1964) is transformed into crystallized MoO_2 by a reduction process:

$$MoO_3 + H_2 \rightarrow MoO_2 + H_2O. \quad (6)$$

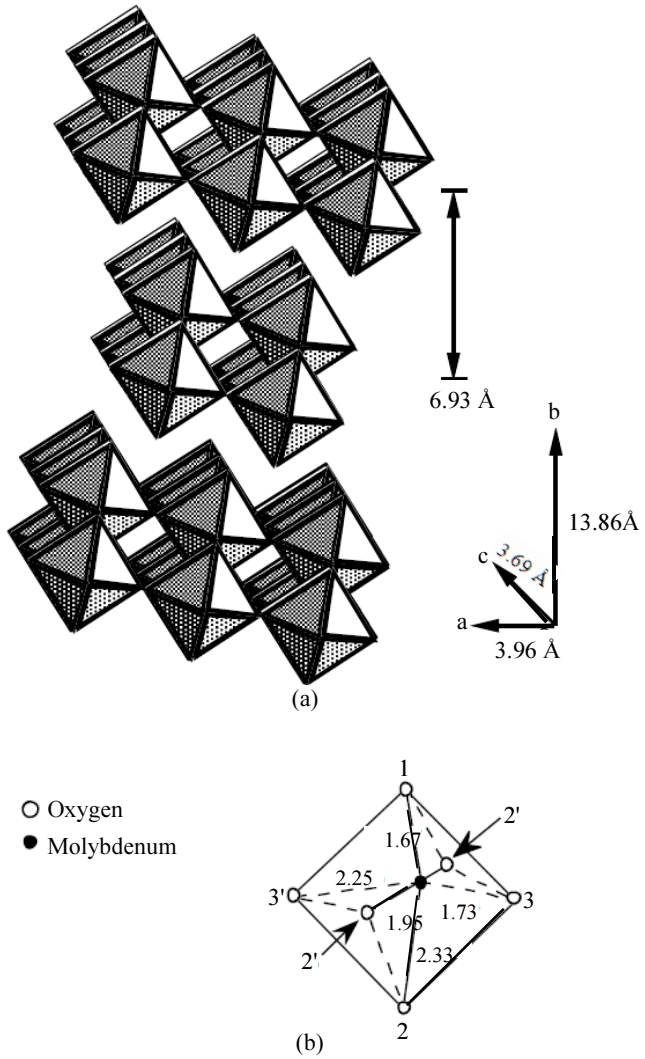

Fig. 8: (a) Layered structural model of α-MoO_3 (b) The co-ordination of oxygen atoms around the molybdenum atoms; (numbers shown are MoO_3 bond lengths in Å)

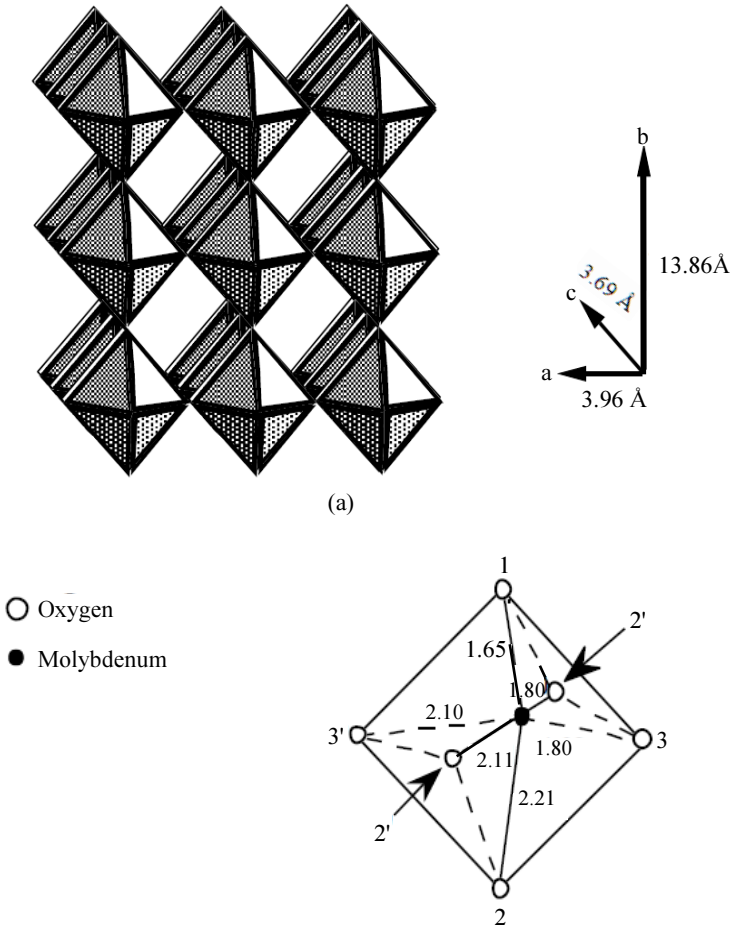

Fig. 9: (a) ReO_3 type structural model of β´-MoO_3. (b). The co-ordination of oxygen atoms around the molybdenum atoms (numbers shown are MoO_3 bond lengths in Å)

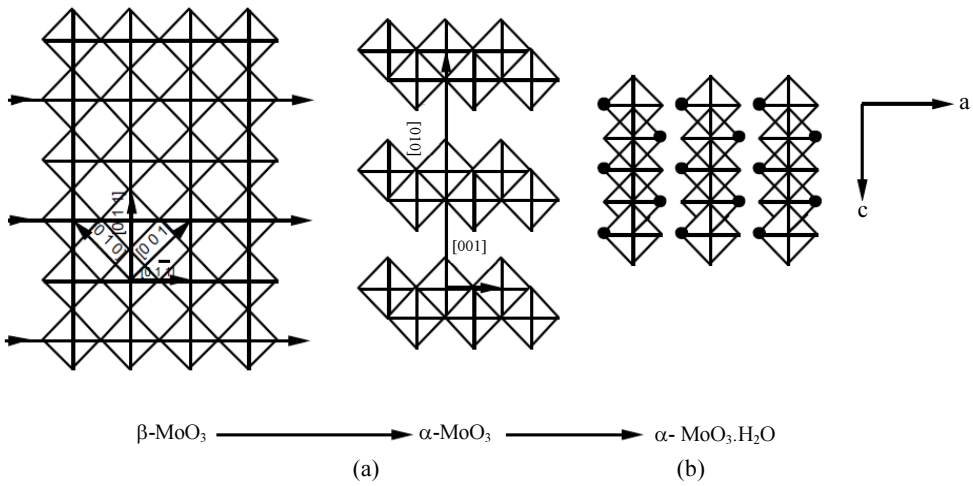

Fig. 10: (a) Structural model for the topotactic transformation of β-MoO_3 to α- MoO_3. (b) Structural model for α- $MoO_3.H_2O$; filled circles indicate co-ordinated H_2O groups

The crystallized black MoO_2 cannot remain stable at room temperature (Ohfuji, 1984; Naguib and Kelly, 1972) and can be rapidly oxidized back to MoO_3 at higher temperature (~1273 K) (Ohfuji, 1984).

In MoO_3 thin film and in its hydrogen molybdenum bronze, Mo-Mo distances are too large to form the metallic bonds, probably due to lack of overlap of 4d-wave functions (Anwar and Hogarth, 1988; Rao *et al*., 2013). Therefore, the electronic and physical properties are interpreted by polaronic excitations and hoppings between Mo^{5+}-Mo^{6+} species.

Refractive Index, Film Density and Electronic Polarizability

Figures 2 and 3 show that the temperature dependent n-values of MoO_3 are monotonically and linearly decreasing. Such behaviour is characteristic for the material in which temperature of the optical indices is associated with thermal expansion which is related to the density of the material.

The density of bulk material or of the film can be calculated from refractive index data using the following well known expression (Born and Wolf, 2013; Jacobson, 1975):

$$\frac{p_f}{p_b} = \frac{n_f^2 - 1}{n_f^2 + 2} \times \frac{n_b^2 + 2}{n_b^2 - 1}, \tag{7}$$

where, ρ_f is the average film density and ρ_b the bulk density; n_f denotes the refractive index of the film and n_b the refractive index of bulk. Inserting the values of ρ_f and ρ_b (Hussain, 2001; 2007) and n_f (from Table 2) into Equation 7, the value of bulk refractive index, n_b of MoO_3 is calculated as 2.7 at 0.633 μm which agrees with the other researchers (Tubbs, 1974; Deb, 1968).

Using the bulk values of n_b as 2.7 and ρ_b as 4.71 gcm^{-3}, we can transform Equation (7) into:

$$\rho_f = 6.96\left[\frac{n_f^2 - 1}{n_f^2 + 2}\right]. \tag{8}$$

The temperature dependent film density data of MoO_3 thin films was derived from Equation (8) using ellipsometric data (Tables 2-4) on MoO_3 over the temperature range 120<T<460 K and are displayed in Figs. 11-13. The experimental curves shown in Fig. 11 indicate that the film density and refractive index of the films decrease with the increase in temperature due to porous nature of the films, but the overall change in mass density (or in the refractive index) in the temperature range 295≤T<460 K is not more than 5% than the room temperature data. Experimental Figs. 2 and 3 also show the same trend over the same temperature range. It is also a fact in the litrature that the optical band gap energy depends on the temperature and it becomes smaller at higher temperature for MoO_3 thin films (Hussain, 2001). It should be noted that the dispersion of the refractive index has already been analysed (Hussain, 2002b) in terms of the E_o (optical band gap) and E_d (dispersion energy) using the single oscillator dispersion model of Wemple and Domenico (1971).

Figure 13 shows that the film density goes on increasing as the temperature decreases from 297 to 120 K. The increase in the refractive index over the same temperature range can be noticed in Fig. 4. This kind of effect could be due to self-trapped charge carriers, known as small polaronic and bipolaronic species which will be explained fully in section D.

Polarizability should be defined before I discuss the relationship between refractive index, film density and polarizability.

The polarization (α_{tot}) is defined as the dipole moment per unit volume, averaged over the volume of a cell and it is the ability for a molecule to be polarized. The total polarizability can be expressed as:

$$\alpha_{tot} = \alpha_e + \alpha_i + \alpha_d, \tag{9}$$

Which is the sum of electronic (α_e), ionic (α_i) and dipolar (α_d) polarizabilities which molecule's internal structure. In the region of visible light, the ionic polarizability (α_i) of any material can be neglected. Because MoO_3 thin film is a non-dipolar (ionic) material, so only the electronic polarizability (α_e) is connected with it over the visible spectral range.

The refractive index (n_f) and film density (ρ_f) are related to electronic polarizability (α_e) through the famous Lorentz-Lorenz relation (Singh *et al*., 2006; Hecht, 2012):

$$\frac{n_f^2 - 1}{n_f^2 + 2} = \left[\frac{4\pi}{3} N_A \frac{\rho_f}{M}\right]\alpha_e. \tag{10}$$

Here, N_A is the Avogadro's number and M is the molecular weight of the material.

Inserting the values of $N_A = 6.023\times10^{23}\ mol^{-1}$ *and* $M = 144\ g\ mol^{-1}$ into Equation (10), the expression for electronic polarizability can be reshaped as:

$$\alpha_e = 5.711 \times \frac{n_f^2 - 1}{n_f^2 + 2} \times 1/p_f. \tag{11}$$

The temperature-dependent-electronic polarizabilities of MoO_3 thin films were calculated from Eq. (11) by the help of refractive index (n_f) data (Tables 2 and 4) and from the film density (ρ_f) data using Eq. (8). The average electronic polarizability of MoO_3 thin films as calculated from Eq. (11) at room temperature is found to be 8.20×10^{-24} cm^3. The measured electronic polarizabilities are represented in Figs. 12 and 14. It is very obvious from Figs. 12 and 14 that the values of electronic polarizability (or depolarization coefficients) of MoO_3 thin films were almost constant over the whole heating and cooling process. This kind of behaviour is characteristic for the materials for which the temperature dependence of the optical indices is associated with thermal expansion (Kang *et al*., 2003). It should be noted that a higher degree of crytallinity in MoO_3 thin films could give rise to a higher electronic polarizability.

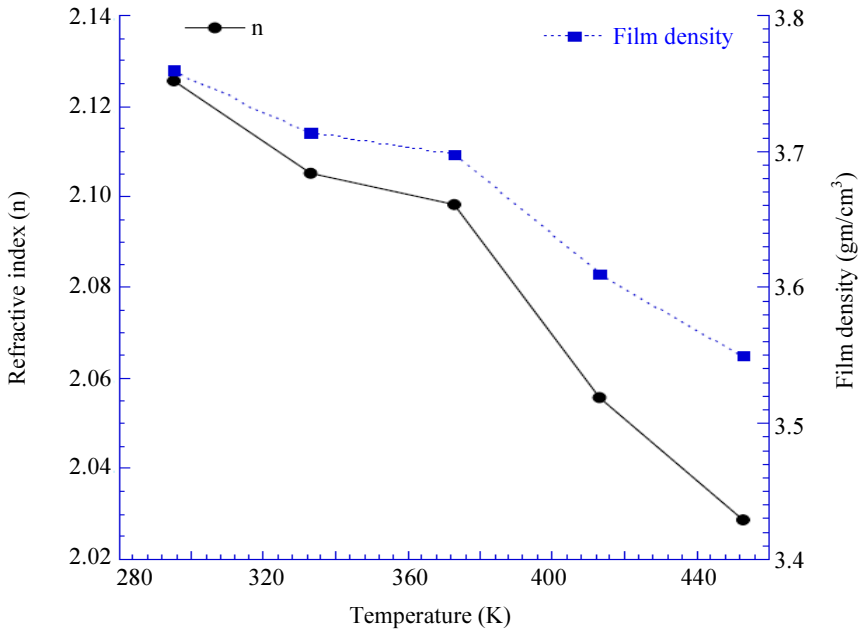

Fig. 11: Plot of refractive index and film density Vs temperature, of MoO_3 thin films in the range 295-460 K

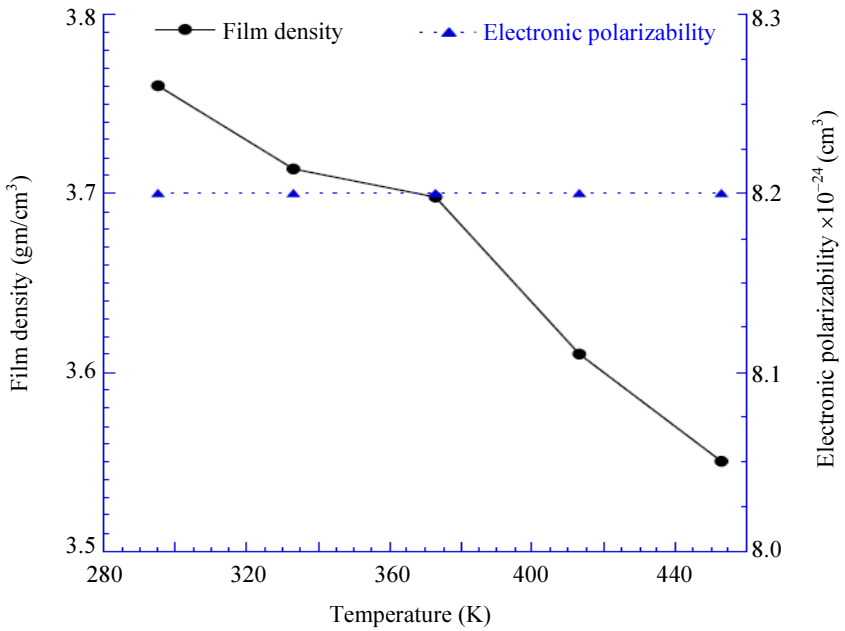

Fig. 12: Film density and electronic polarizability Vs temperature, of MoO_3 thin films in the range 295-460 K

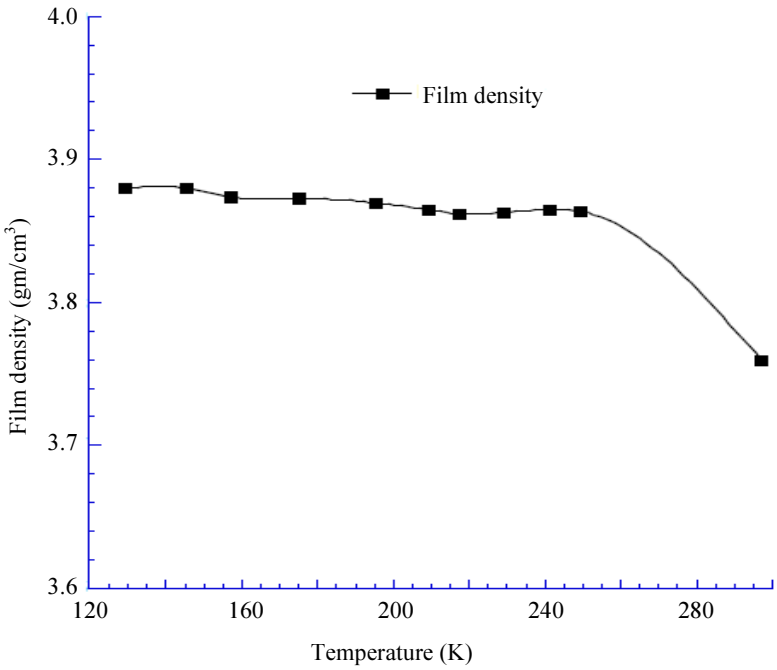

Fig. 13: Film density Vs temperature, of MoO_3 thin film in the range 120-300 K

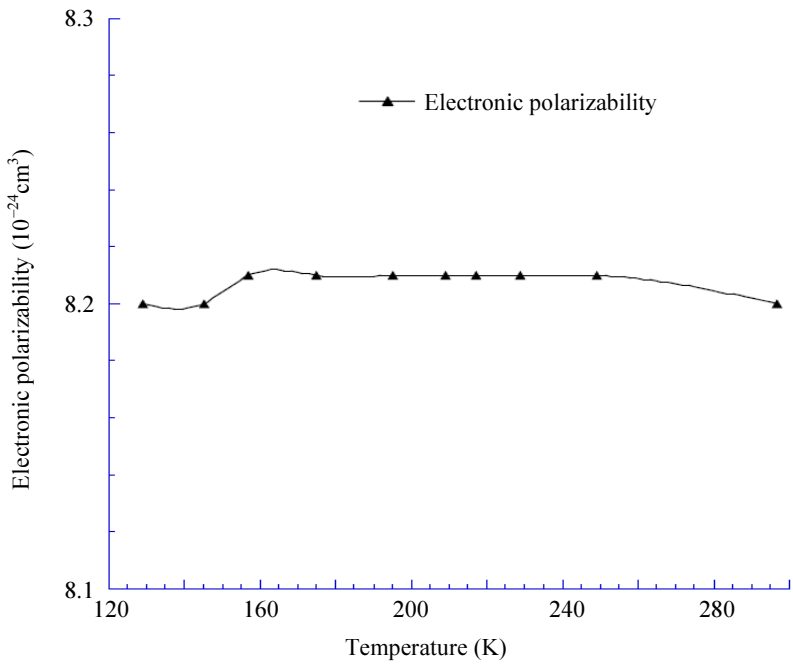

Fig. 14: Electronic polarizability Vs temperature, of MoO_3 thin film in the range 120-295 K

Thermo-Optic Coefficients and Interpretations

Values of n obtained at λ=0.633 μm at room temperature were found to have a small range from 2.12 to 2.13 for the reported evaporated MoO_3 thin films; and this range is very close to the refractive index (n), as found in Fig. 15 using spectrophotometric technique. It is also in agreement with other reseachers (Tubbs, 1974; Hussain, 2001; Carcia *et al*., 1987; Abdellaoui *et al*., 1988). The k-values determined at room temperature are found to be in the range from 0.004 to 0.006 which are due to slight blue colouration in the reported films. This range is also comparable with the values shown in Fig. 15. It also agrees with the others in the

literature (Tubbs, 1974; Hussain, 2001; Abdellaoui *et al*., 1988). The p-d band gap of MoO_3 thin films has been found within a range 3.05-3.07 eV (Hussain, 2001; 2007), which also agrees with other workers (Miyate and Akiyoshi, 1985; Rabalais *et al*., 1974).

For a specific wavelength, the index with the increased (or decreased) temperature could be expressed as:

$$n_2 = n_1 + \frac{dn}{dT}(T_2 - T_1), \quad (12)$$

Or:

$$\frac{dn}{dT} = \frac{n_2 - n_1}{T_2 - T_1}, \quad (13)$$

where, n_2 is the refractive index at temperature T_2 (higher or lower than T_1), n_1 is the refractive index at T_1 and dn/dT is the Thermo Optic Coefficient (TOC) normally used in opto-electronic devices.

In the first step, TOC_s (dn/dT and dk/dT) of MoO_3 thin films over the range 295-460 K are calculated from Tables 2 and 3. We have developed the mathematical formulations for temperature-dependent refractive index data and the associated thermo optic coefficients, TOCs. The following are the mathematical equations which fit to the reported temperature dependent n and k data:

$$n(T) = n_0 + B_n(T - T_0), \quad (14)$$

$$k(T) = k_0 + D_k(T - T_0). \quad (15)$$

In Eq. (14), n_0 and T_0 are initial values (room temperature values) and n and T are any choosen (or final) values of refractive index and temperature. B_n is taken as an average value of dn/dT associated with reported MoO_3 thin films with some $\pm$ standard deviation. Similarly, in Eq. (15), k_0 and T_0 are initial values (room temperature values) and k and T are any choosen (or final) values of extinction coefficient and temperature. The value of D_k is taken as an average of dk/dT associated with the temperature dependent k-data of reported MoO_3 thin films with somestandard deviation.

In Table 2, thermo-optic coefficients (TOCs): dn/dT varies from -7.86×10^{-4}/K at 373 K to 3.65×10^{-4}/K at 297 K and dk/dT varies from -1.385×10^{-5}/K at 373 K to 9.1×10^{-6}/K at 297 K, but this data cann't be fitted to Eqs. (14) and (15) due to anomalous behaviour of n and k.

Thermo-optical coefficients (dn/dT) relating to MoO_3 thin film as determined from Table 3 are found to be negative in the visible part of spectral range and have values in the range from -6.24 to -0.291×10^{-4} K^{-1} over the temperature range 295-460 K. Similarly, dk/dT values for MoO_3 determined from Table 3 are all positive and range from 0.1 to 3.1×10^{-5} K^{-1} over the same temperature range.

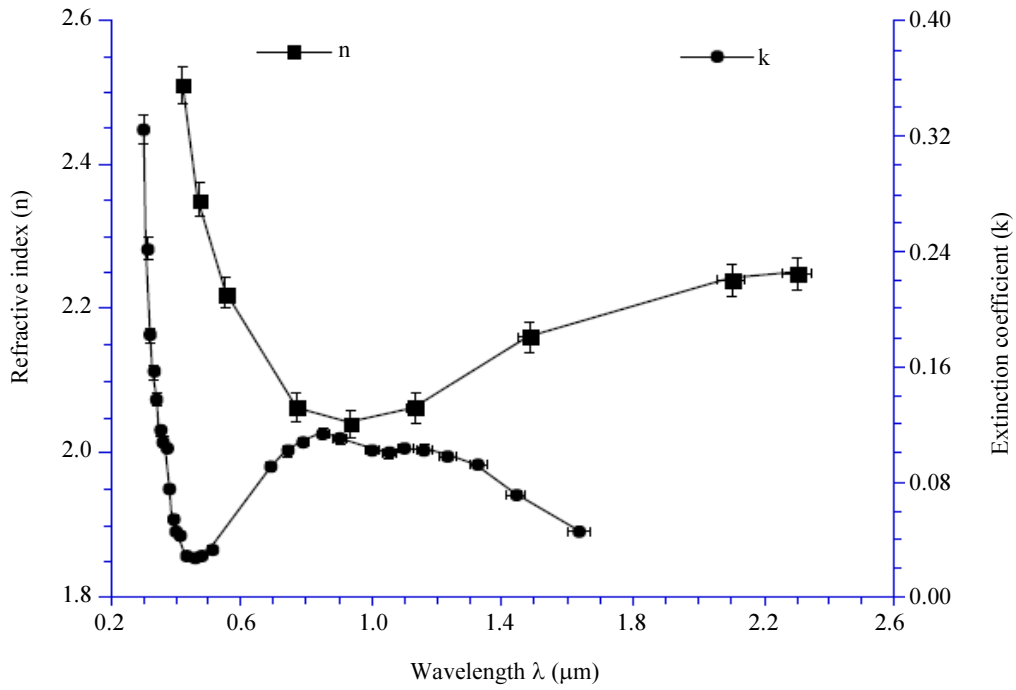

Fig. 15: Plot of optical constants (n, k) Vs wave length (λ), of slightly coloured MoO_3 thin film

The values of dn/dT and dk/dT (TOCs) as determined from Table 3 (or measured from slopes of curves in Fig. 3) can be fitted to Eqs. (14) and (15) as:

$$n(T) = 2.1273 + B_n\left(T - T_0\right), \tag{16}$$

where, $n_o = 2.1273$ and $B_n = [-3.265 \pm 2.974] \times 10^{-4}\, K^{-1}$. And:

$$k(T) = 0.0058 + D_k\left(T - T_0\right), \tag{17}$$

where, $k_o = 0.0058$ and $D_k = [1.60 \pm 1.50] \times 10^{-5}\, K^{-1}$.

Equations (16) and (17) fit well to the reported ellipsometric data within a relative accuracy of ±10.

TOCs calculated from Tables 3 are very close to the values reported in the literature (Hussain, 2001; Martinez *et al*., 2013; Torres *et al*., 2005). The small changes in TOCs are due to small changes in the electronic polarizability in the range 295-460 *K* (Fig. 12). It is clearly visible from Fig. 12 that after heating in the above temperature range, the new values of optical constants of MoO_3 are not close to their initial values. So it is an irreversible process showing an unclosed thermal hysteresis for the heating cycles of the films.

Figures 2 and 3 indicate that on simple heating up to 453 K, MoO_3 thin films start becoming more transparent instead of losing more oxygen. Figure 2 shows an increase in the index of absorption (or conductivity) with increasing temperature. It is interpreted by the fact that in an oxygen deficient MoO_3 thin films, a number of oxygen vacancies act as donors and are capable of capturing one or two electrons per donor, from where electrons are ionized thermally as well as optically and eventually cause an increase in the optical and electrical conductivity.

Table 5 gives the TOCs: dn/dT changes from -5.59×10^{-4}/K at 413 K to -5.66×10^{-4}/K when annealed at 413 K for 14 h; and dk/dT changes from 2.84×10^{-5}/K at 413 K to 1.644×10^{-5}/K when annealed at 413 K for 14 h. Similarly, TOCs from Table 6 reflects that dn/dT changes from -3.51×10^{-4} to -8.45×10^{-5}/K when annealed at 453 K for 11 h and changes to -7.4×10^{-4}/K when annealed with oxygen plasma for further 25 h; and dk/dT changes from initial 1.019×10^{-4} to final 4.582×10^{-4}/K under the same conditions. These small changes in TOCs indicate that the reported MoO_3 films still remain microcrystalline even after being annealed at 453 K for so long time.

During annealing mode, a lot of outgassing is involved mostly due to evolution of water which is present in the form of H_2MoO_4 on the surface, but also in the form of great loss of oxygen from MoO_3 thin films. Annealing certainly helps in reducing the porosity with a minor rearrangement in the Mo-O bond lengths, but produces irreversible changes in the morphology of the films. Vacuum-annealing and oxidative-annealing give open hysteresis loops as shown in Figs. 5 and 6 and these irreversible results do not appear to bleach any sample in accordance with the following relations (Sian *et al*., 2004):

$$MoO_{3-y}\left(OH\right)_x + \frac{y}{4}O_2 \rightarrow MoO_3 + \frac{y}{2}H_2O, \tag{18}$$

And:

$$Mo_2O_5 + \frac{1}{2}O_2 \rightarrow 2MoO_3. \tag{19}$$

The cause of this irreversibility is a partial reduction and also because of presence of hydroxy group in the films. In the case of annealing process, optical or electrical conduction can occur by the hopping mechanism between different oxidation states (e^- moving from M^{5+} or $M^{4+} \rightarrow M^{6+}$) (Sian *et al*., 2004; Torres *et al*., 2005). The oxidation of MoO_x converts Mo^{5+} (or Mo^{4+}) to Mo^{6+} and also reduces the oxygen vacancy concentration, thereby increases the optical transmittance and electrical resistivity of the films. The optical modulation of the reported films is increased from 4 to 9% with increase of annealing temperature from 373 to 453 K. The optical modulation mainly depends on the quantity of H^+ insertion into the films during annealing. The films annealed at 453 K show good optical modulation and that may be due to more insertion of H^+ ions into the films because of growth of columnar structure of the films.

After exposure to oxygen plasma, the colour of the sample becomes black due to significant amount of Mo^{4+} species in the sample with more annealing at higher temperatures, further reduction and additional defect structure can be produced in the film with ultimately a new stable crystallographic phase, probably a rhombic phase (Pardo and Torres, 2012). A single phase orthorhombic α-MoO_3 films could only be obtained by annealing the films at temperature above 673 K (Madhavi *et al*., 2013; Pardo and Torres, 2012).

Thermo optical properties of MoO_3 thin films during cooling cycles over the temperature range 120<T<300 K are represented in Table 4. Thermo-optical coefficients (dn/dT) relating to MoO_3 thin film as determined from Table 4 are found to be negative in the visible part of spectral range and have values in the range from -3.643 to $-3.29\times10^{-4}K^{-1}$ over the temperature range 120-300 K. Similarly, dk/dT values for MoO_3 determined from Table 4 are all positive and range from 7.792 to $7.77\times10^{-5}\,K^{-1}$ over the same temperature range.

TOCs calculated from Table 4 (or measured from the slopes of curves in Fig. 4) can be fitted to Eqs. (14) and (15) as:

$$n(T) = 2.1240 + B_n\left(T - T_0\right), \tag{20}$$

where, $n_o = 2.1240$ and $B_n = [-3.47 \pm 0.18] \times 10^{-4}\, K^{-1}$.
And:

$$k(T) = 0.01592 + D_k\left(T - T_0\right), \tag{21}$$

where, $k_o = 0.01592$ and $D_k = [7.78 \pm 0.011] \times 10^{-5}\, K^{-1}$.

Equations (20) and (21) fit well to the experimental ellipsometric data within a relative accuracy of ±10.

It is interesting to note that the thermal treatment over the temperature range 297-129 K is virtually reversible. The values of n and k, which form closed hysteresis loops, can be perceived in Fig. 4. It is important to note that these small changes in TOCs are due to small changes in the values of electronic polarizability during the cooling cycles (Fig. 14).

The shifts in the optical constants are obviously related to the changing of the conductance of the sample during cooling processing. When the temperature goes down to 129 K the conductivity reaches its lowest value and when the temperature increases, so does the conductivity but in a slightly different way. When the sample returns to room temperature, it appears again slightly blue. The mechanism of conduction in amorphous or microcrystalline solids is believed to be due to electronic hoppings through localized levels. The localized levels are donor-like or trap-like, depending on their ability to donate or accept electrons and the position of the Fermi level depends critically on the respective distributions of donor-like or trap-like levels.

The traps are likely to spread over a broader range of energies than donors or acceptors. The degree of overlap of the donor-like (or trap-like) levels vary widely, as observed by the fact that the k-values of MoO_3 thin films vary vastly during cooling treatment. For example, as is observed in Fig. 4, the trend in the k-plot manifests metal-insulator transition features over the temperature range 200-130 K, but there are no indication of Peirels transitions (Rao *et al*., 2013; Pergament *et al*., 2014) in the investigated temperature range.

Polaronic and Bipolaronic Excitations in MoO_3 Thin Films

MoO_3 is one of the transition metal oxides which are known to have large dipole moments due to large difference between the static dielectric constant and the high frequency dielectric constant value. With such a large difference, the charge carriers are almost self-trapped small polarons or bipolarons and evidence that photo (or thermo) excited electrons and holes do so in transition metal oxides has been reported by several researchers (Gehlig and Salje, 1983; Eagles, 1984; Lakhno, 2013). Fresh MoO_3 thin film experiences some thermal decomposition during evaporation resulting in lower valence Mo^{5+} and Mo^{4+}states (Dasgupta *et al*., 2015; Peelaers *et al*., 2017; Mrowiecka *et al*., 2008). ESR (Deb, 1968; Anwar *et al*., 1989), XPS (Peelaers *et al*., 2017; Maruyama and Kanagawa, 1995; Santhosh *et al*., 2017) and NMR (Santhosh *et al*., 2017; Ritter *et al*., 1985) measurements show that the localization of surplus electrons is on Mo ions and not on the oxygen vacancies. We also believe that in the sub-stiochiometric oxide thin film (WO_3, MoO_3, etc) the charge carrier bound to the W or Mo ion is also strongly coupled to the lattice optical phonons, causing a lattice distortion around the host metallic ion. Since the optical phonon frequencies in metal oxides are usually high 0.05-0.16 eV (Svensson *et al*., 1988; Pardo and Torres, 2012; Gehlig and Salje, 1983) and the polaronic binding energy is also sizable E_p = 0.2-0.4 (Gehlig and Salje, 1983; Eagles, 1984; Devreese and Alexandrov, 2009), thus the permitted value for the unfilled electronic band could be of the order of 0.5-1.0 eV (Mott and Davis, 1979; Arfaoui *et al*., 2015), which is large enough for the small polaron formation.

During any higher temperature or annealed state of MoO_3 thin film, generally, polaron jump from different lower valence states (Mo^{4+}, Mo^{5+}) to the neighbouring higher valence Mo^{6+} states on the basis of a variable-range hopping mechanism (Mott and Davis, 1979; Tahini *et al*., 2016; Gesheva *et al*., 2005). The shape of the polaron band goes on changing during heating and annealing cycles and the suitability about the type of polaron model in a particular annealing mode may arise because of the simultaneous presence of two types of polaron. Either small polarons hop as almost independent species or can coexist with the large-radius polarons to form delocalized states (Mott and Davis, 1979; Tahini *et al*., 2016) during annealing at higher temperatures. However, a rigorous theoretical treatment is needed in order to interpret the experimental data and to clarify about the applicability of proper polaron theory.

During cooling, colouration (or conductance) change is caused either by small polarons (Lakhno, 2013; Tahini *et al*., 2016) or by the excitation of bipolaronic entities (Mo^{5+}-Mo^{5+}) (Devreese and Alexandrov, 2009; Arfaoui *et al*., 2015). Assemblage and disassemblage of bipolarons (Mo^{5+}-Mo^{5+}) is shown in Fig. 16.

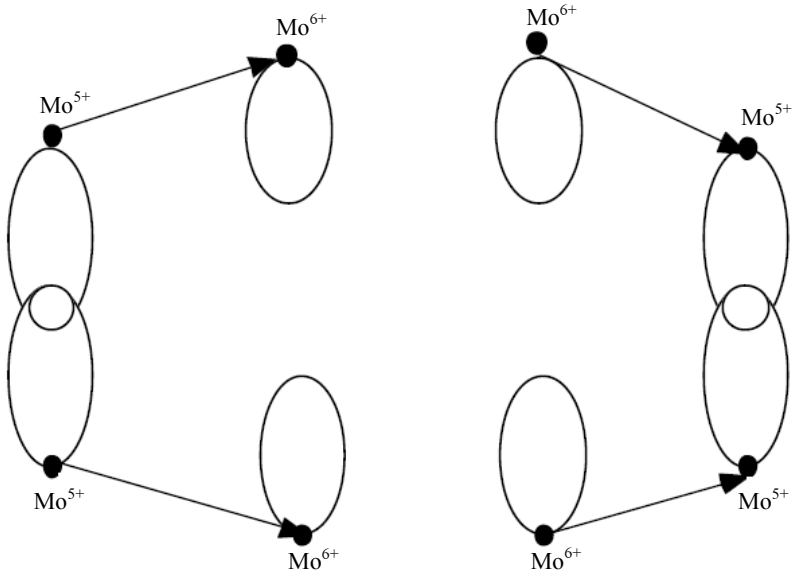

Fig. 16: Simple sketch of bipolaron model

The bipolaronic entities (Mo^{4+}-Mo^{4+}) might also exist during the cooling process (Gesheva *et al*., 2005). In the case of bipolaronic state, a short-range coulomb repulsion (intersite) should be below 1 eV to ensure bipolaron formation and it is quite possible because the high-frequency or short-range dielectric constant in metal oxides is usually large. A bipolaron will be energetically stable, if the static dielectric constant $\varepsilon_o$and polaron binding energy E_b are sufficiently large and obey the condition such that bipolaron binding energy E_{bi} (R)<2 E_b (R) (Mott and Davis, 1979; Arfaoui *et al*., 2015; Alexandrov and Devreese, 2009). Since polarons and bipolarons in the case of transition metal oxides are formed well above the superconductivity transition temperature T_c, so the reported low temperature data also need to be carefully analyzed either mostly within the picture of polaron or bipolaron or both.

Summary and Conclusion

Freshly evaporated MoO_3 thin films prepared on unheated substrates are always microcrystalline in structure. Moreover, in our case, the prepared films were slightly blue either due to deficiency in oxygen or due to water, or because of hydroxyl groups.

The reported temperature dependent ellipsometric data on MoO_3 thin films was computed to calculate optical constants n and k over the temperature range 120<T<460 K. We also measured mass densities, thermo optic coefficients (TOCs) and electronic polarizabilities of MoO_3 thin films over the same temperature range. Thermo-optical coefficients (dn/dT) relating to MoO_3 thin film are found to be negative in the visible part of spectral range and have values in the range from -6.24 to -0.291×10^{-4} K^{-1} over the temperature range 295-460 K. Similarly, dk/dT values determined for MoO_3 are all positive and range from 0.1 to 3.1×10^{-5} K^{-1} over the same temperature range. These tiny changes in TOCs are due to small changes in the values of electronic polarizability (α_e), which were calculated in the range from 8.203 to 8.205×10^{-24} cm^3 over the temperature range 295-460 K.

Vacuum-heating and oxidative-annealing certainly removes a lot of water and definitely helps to reduce the porosity, but assists little towards bleaching process in the reported temperature range 295-460 K. Consequently our experimental annealing runs produce minor rearrangement in the Mo-O bond lengths, but create a lot ofirreversiblechanges in the morphology of the films.

For the cooling cycles, the values of dn/d for MoO_3 thin films are also found to be negative in the visible part of spectral range and have values in the range from -3.643 to -3.29×10^{-4} K^{-1} over the temperature range 120-300 K. Similarly, dk/dT values for MoO_3 are found to be all positive and range from 7.792 to 7.77×10^{-5} K^{-1} over the same temperature range. These meagre changes in TOCs are due to little changes in the values of electronic polarizability (α_e), which were found to be in the range from 8.203 to 8.20×10^{-24} cm^3 over the temperature range 120-300 K.

In the case of cooling runs, different lower values of k were obtained during different cooling cycles, but most of the k-values returned to original when MoO_3 thin films were back to room temperature. So, for the cooling cycles, the hysteresis loops are closed for the investigated ellipsometric data. This means that the

thermal treatment in the temperature range 120 to 300 K is definitely reversible.

The reported ellipsometric data on MoO_3 thin films is also interpreted in terms of excitations of polarons and bipolarons. Briefly, Room temperature and higher temperature excited electronic states correspond to hopping of polarons from their donor states to the immediate neighbouring higher energetic impurity states within the polaron band. Similarly the changes in the conductivity and other film characteristics during cooling are caused either by polaronic or bipolaronic or mixed excitations.

We hope that this study will stimulate more theoretical work with a view to polaron and bipolaron theory.

Acknowledgment

This research was done in the EEE department at Imperial College London by private fundings. The author would like to acknowledge the invaluable assistance provided by the technicians of the EEE laboratories.

Funding Information

Sampling and experimental process were financially supported by the author.

Ethics

This article is original and contains unpublished material. Author declares that there is no ethical issue and no conflict of interest that may arise after the publication of this manuscript.

References

Gesheva, K.A., T.M. Ivanova and G. Bodurov, 2012. Transition metal oxide films: Technology and "Smart Windows" electrochromic device performance. Progress Organic Coat., 74: 635-639. DOI: 10.1016/j.porgcoat.2011.07.016

Hsu, C.S., C.C. Chan, H.T. Huang, C.H. Peng and W.C. Hsu, 2008. Electrochromic properties of nanocrystalline MoO_3 thin films. Thin Solid Films, 516: 4839-4844. DOI: 10.1016/j.tsf.2007.09.019

Scrosati, B.,1990. Second International Symposium on Polymer Electrolytes. Elsevier Applied Science, ISBN-10: 1851664734, pp: 482.

Granqvist, C.G., 2014. Electrochromics for smart windows: Oxide-based thin films and devices. Thin Solid Films, 564: 1-38. DOI: 10.1016/j.tsf.2014.02.002

Tubbs, M.R., 1974. MoO_3 layers-optical properties, colour centres and holographic recording. Phys. Stat. Sol., 21: 253-260. DOI: 10.1002/pssa.2210210127

Anwar, M. and C.A. Hogarth, 1988. Effects of film thickness and substrate temperature on DC conduction in thin amorphous films of MoO_3. Phys. Stat. Sol., 109: 419-436. DOI: 10.1080/00207218908925399

Matsushina, T., Y. Kinashita and H. Murata, 2007. Formation of ohmic hole injection by inserting an ultrathin layer of molybdenum trioxide between indium thin oxide and organic hole-transporting layers. Appl. Phys. Lett., 91: 253504. DOI: 10.1063/1.2825275

You, H., Y. Dai, Z. Zhang and D. Ma, 2007. Improved performances of organic light-emitting diodes with metal oxide as anode buffer. J. Appl. Phys., 101: 026105-026110. DOI: 10.1063/1.2430511

Haitao, X. and Z. Xiang, 2013. Investigation of hole injection enhancement by MoO_3 buffer layer in organic light emitting diodes. J. Appl. Phys., 114: 244505. DOI: 10.1063/1.4852835

Chu, C.W., S.H. Li, C.W. Chen, V.S. Triya and Y. Yang, 2005. High-performance organic thin-film transistors with metal oxide/metal bilayer electrode. Appl. Phys. Lett., 87: 193508. DOI: 10.1063/1.2126140

Kumaki, D., T. Umeda and S. Tokito, 2008. Reducing the contact resistance of bottom-contact pentacene thin-film transistors by employing a MoO_x carrier injection layer. Appl. Phys. Lett., 92: 013301. DOI: 10.1063/1.2828711

Shrotriya, V., G. Li, Y. Yao, C.W. Chu and Y. Yang, 2006. Transition metal oxides as the buffer layer for polymer photovoltaic cells. Appl. Phys. Lett., 88: 073508.

Tseng, Y.C., A.U. Mane, J.W. Elam and S.B. Darling, 2012. Ultrathin molybdenum oxide anode buffer layer for organic photovoltaic cells formed using atomic layer deposition. Sol. Energy Mater. Sol. Cells, 99: 235-239.

Zhang, M., Irfan, H. Ding, Y. Gao and C.W. Tang, 2010. Organic schottky barrier photovoltaic cells based on MoO_x/C_{60}. Appl. Phys. Lett., 96: 183301.

Hori, T., T. Shibata, V. Kittichungchit, H. Moritou and J. Sakai *et al*., 2009. MoO_3 buffer layer effect on photovoltaic properties of interpenetrating heterojunction type organic solar cells. Thin Solid Films, 518: 522-525.

Rao, M.C., K. Ravindranadh, A. Kasturi and M.S. Shekhawat, 2013. Structural stoichiometry and phase transitions of MoO_3 thin films for solid state micro-batteries. Res. J. Recent Sci., 2: 67-73.

Cheng, W., F. Li, Z. Tao and J. Chen, 2006. Vapour-transportation preparation and reversible lithium intercalation/deintercalation. J. Phys. Chem. B., 110: 119-124.

Manivel, A., G.J. Lee, C.Y. Chen, J.H. Chen and S.S. Ma *et al*., 2015. Synthesis of MoO_3 nanoparticles for Azo dye degradation by catalytic ozonation. Mater. Res. Bull., 62: 184-191.

Chen, Y., C. Lu, L. Xu, Y. Ma and J.J. Zhu *et al*., 2010. Single-crystalline orthorhombic Molybdenum oxide nanobelts: Synthesis and photocatalytic properties. Cryst. Eng. Comm., 12: 3740-3747.

Bai, S., C. Chen, Y. Tian, S. Chen and C.C. Liu *et al*., 2015. Facile synthesis of α-MoO_3 nanorods with high sensitivity to Co and intrinsic performance. Mater. Res., 64: 252-256.

Khojier, K., H. Savaloni and S. Zolghadr, 2014. On the dependence of structural and sensing properties of sputtered MoO_3 thin films on argon gas flow. Appl. Surf. Sci., 320: 315-321.

Touihri, S., S.A. Arfaoui, Y. Tarchouna, A. Labidi and J.C. Bernede *et al*., 2017. Annealing effect on physical properties of evaporated molybdenum oxide thin films for ethanol sensing. Appl. Surf. Sci., 394: 414-424.

Prasad, A.K., D.J. Kubinski and P.I. Gouma, 2003. Comparison of sol-gel and ion beam deposited MoO_3 thin film gas sensors for selective ammonia detection. Sensors Actuators B., 93: 25-30.

Hosono, K., I. Matsubara, N. Murayama, S. Woosuck and N. Izu, 2005. Synthesis of polypyrrole/MoO_3 hybrid thin films and their volatile organic compound gas-sensing properties. Chem. Mater., 17: 349-354.

Wang, J., K.C. Rose and C.M. Lieber, 1999. Load-independent friction: MoO_3 nanocrystal lubricants. J. Phys. Chem. B., 103: 8405-8409.

Bertrand, O., N. Floquet and D. Jacquot, 1985. The crystallographic shear planes of the non-stoichiometric molybdenum oxides as revealed by RHEED: Investigation from the $Mo_{18}O_{52}$ (100) surface. Surf. Sci., 164: 305-319.

Punitha, K., R. Sivakumar and C. Sanjeeviraja, 2014. Pulsing frequency induced charge in optical constants and dispersion energy parameters of WO_3 films grown by pulsed direct current magnetron sputtering. J. Appl. Phys., 115: 113512.

Schollhorn, R., R. Kuhlmann and J. O. Besenhard, 1976. Topotactic redox reactions and ion exchange of layered MoO_3 bronzes. Mat. Res. Bull., 11: 83-90.

Li, Y., D. Wang, Q. An, B. Ren and Y. Yao *et al*., 2016. Flexible electrode for long life rechargeable sodium-ion batteries: Effect of oxygen vacancy in MoO_{3-x}. J. Mater. Chem. A., 4: 5402-5405.

Wang, X.J., R. Nesper, C. Villevieille and P. Novak, 2012. Ammonolyzed MoO_3 nanobelts as novel cathode material of rechargeable Li-ion batteries. Adv. Energy. Mater., 3, 606-614.

Madhavi, V., P. Kondaiah, S.S. Rayudu, O.M. Hussain and S. Uthanna, 2013. Properties of MoO_3 films by thermal oxidation: Annealing induced phase transition. J. Mater. Express, 3: 135-143.

Svensson, J.S.E.M., D.K. Benson and C.E. Tracy, 1988. Temperature dependent optical absorption in electrochromic tungsten and molybdenum oxides. SPIE., 1016: 19-28.

Hussain, Z., 2002b. Optical and Electrochromic properties of annealed lithium-molybdenum-bronze thin films. J. Electron. Mater., 31: 615-629.

Colaitis, D., 1991. Microstructural aspect of electron transfer in the blue and red molybdenum bronzes. Phys. Stat. Sol., 165: 157-173.

Sian, T.S. and G.B. Reddy, 2004. Optical, structural and photoelectron spectroscopic studies on amorphous and crystalline molybdenum oxide thin films. Sol. Energy. Mater. Sol. Cells, 82: 375-386.

Hussain, Z., 2018a. Optical constants and electrochromic characteristics of M_xWO_3 bronzes. Appl. Opt., 57: 5720-5732.

Hussain, Z., 2018b. Optical constants and electrochromic characteristics of H_xMoO_3 and Li_xMoO_3 Bronzes. J. OSA A., 35: 817-829.

Hussain, Z., 1999. Vacuum temperature-dependent ellipsometric studies on WO_3 thin films. Appl. Opt., 38: 7112-7127.

McEvoy, T.M. and K.J. Stevenson, 2003. Electrochemical preparation of molybdenum trioxide thin films: Effect of sintering on electrochromic and electroinsertion properties. Langmuir, 19: 4316-4326.

Sian, T.S., G.B. Reddy and S.M. Shivaprasad, 2004. Study of Mg ion intercalation in polycrystalline MoO_3 thin films. Jpn. J. Appl. Phys., 43: 6248-6252.

Azzam, R.M.A. and N.M. Bashara, 1977. Ellipsometry and Polarized Light. 1st Edn., North-Holland, Amsterdan, ISBN-10: 0720406943, pp: 529.

Tiwald, T., 2016. Introduction to ellipsometry: Theory and Applications. J.A. Woollam.

Hussain, Z., 2007. Ph.D. Thesis, University of London.

Evans, H.I., 1987. Ph.D. Thesis, University of London.

Shiojiri, M., T. Miyano and C. Kaito, 1979. Electron microscopic studies of structure and crystallization of amorphous metal oxide films. Jap. J. Appl. Phys., 18: 1937-1947.

Julien, C., A. Khelfa, O.M. Hussain and G.A. Nazri, 1995. Synthesis and characterization of flash-evaporated MoO_3 thin films. J. Crystal Growth, 156: 235-244.

McCrackin, F.L., 1969. NBS technical note 479. U.S. Government Printing Office, Washington.

Itoh, M.M., K. Hayakawa and S. Oishi, 2001. Optical properties and electronic structures of layered MoO_3 Single crystals. J. Phys: Condensed Mater., 13: 6853-6865.

Parise, J.B., E.M. McCarron and A.W. Sleight, 1987. A new modification of ReO_3-type MoO_3 and the deuterated interaction compound from which it is derived: $D_{0.99}MoO_3$. Mat. Res. Bull., 22: 803-811.

Baker, S.C. and P.G. Dickens, 1989. Qualitative bonding models for some molybdenum oxide phases. Solid St. Ionics, 32: 219-227.
DOI: 10.1016/0167-2738(89)90225-7

Dickens, P.G., J.J. Birtill and C.J. Wright, 1979. Elastic and inelastic neutron studies of hydrogen molybdenum Bronzes. J. Solid State Chem., 28: 185-193.

Scanlon, D.O., G.W. Watson, D.J. Payne and D.S.L. Law *et al*., 2010. Theoretical and experimental study of the electronic structures of MoO_3 and MoO_2. J. Phys. Chem. C., 114: 4636-4645.

Diaz, C., V. Lavayen and C. Dwyer, 2010. Single-crystal micro and nano structures and thin films of lamellar Molybdenum oxide by solid state pyrolysis of organometallic derivatives of a cylotriphosphazene. J. Solid St. Chem., 183: 1595-1603.

Kuzmin, A. and J. Purans, 1993. A new fast spherical approximation for calculation of multiple-scattering contributions in X-ray absorption fine structure and its application to ReO_3, $NaWO_3$ and MoO_3. J. Phys: Condens. Mater., 5: 267-282.

Carcia, P.F. and E.M. McCarron, 1987. Synthesis and properties of thin film polymorphs of molybdenum Trioxide. Thin Solid Films, 155: 53-63.

Gunter, J.R., 1972. Topotactic dehydration of molybdenum trioxide hydrates. J. Solid St. Chem., 5: 354-359.

Sabhapathi, V.K., O.M. Hussain, P.S. Reddy, K.T. Ramakrishna and P.J. Reddy, 1995. Optical absorption studies in molybdenum trioxide thin films. Phys. Stat. Sol., 148: 167-173.

Kihlborgn, L. and A. Magneli, 1955. On the thermal decomposition of molybdenum trioxide in vacuo. Acta Chem. Scand., 9: 471-474.

Bursill, L.A., 1969. Crystallographic shear in molybdenum trioxide. Proc. R. Soc. Lond. A., 311: 267-290.

Ohfuji, S.I., 1984. Oxygen concentration changes in oxygen-doped molybdenum films under high temperature annealing. Thin Solid Films, 15: 299-307.

Hansen, S. and A. Andersson, 1988. Electron microscopy of some molybdenum oxide phases after use as catalysts in oxidative ammonolysis and ammoxidation of toluene. J. Solid St. Chem., 75: 225-243.

Kumada, F., M. Okamoto, M. Baba and T. Ikeda, 1986. MoO_3 electron resist and its application to fabrication of Mo fine pattern. Jpn. J. Appl. Phys., 25: L574-L577.

Kihlborg, L., 1959. Studies on molybdenum oxides. Acta Chem. Scand., 13: 954-962.

Epifani, M., P. Imperatori, L. Mirenghi, M. Schioppa and P. Siciliano, 2004. Synthesis and characterization of MoO_3 thin films and powders from a molybdenum chloromethoxide. Chem. Mater., 16: 5495-5501.

So, F.C.T., E. Kolawa, S.C.W. Nieh, X. Zhao and M. Nicolet, 1988. Properties of reactivity sputtered $Mo_{1-x}O_x$ films. Appl. Phys. A., 45: 265-270.

Wold, A., W. Kunnmann, R.J. Arnott and A. Ferretti, 1964. Preparation and properties of sodium and potassium molybdenum bronze crystals. Inorg. Chem., 3: 545-547.

Naguib, H.M. and R. Kelly, 1972. On the increase in the electrical conductivity of MoO_3 and V_2O_5 following ion bombardment. Studies on bombardment-enhanced conductivity-I. J. Phys. Chem. Solids, 33: 1751-1759.

Born, M. and E. Wolf, 2013. Principles of Optics: Electromagnetic Theory of Propagation, Interference and Diffraction of Light. 6th Edn., ISBN-10: 148310320X, pp: 836.

Jacobson, R., 1975. Physics of thin films, Academic, New York.

Deb, S.K., 1968. Physical properties of a transition metal oxide: Optical and photoelectric properties of single crystal and thin film molybdenum trioxide. Proc. R. Soc. Lond. A., 304: 211-231.

Hussain, Z., 2001. Optical and electrochromic properties of heated and annealed MoO_3 thin films. J. Mater. Res., 16: 2695-2707.

Hussain, Z., 2002a. Dopant-dependent reflectivity and refractive index of microcrystalline H_xWO_3 and Li_xWO_3 bronze thin films. Appl. Opt., 41: 6708-6724.

Wemple, S. H. and M.D. Domenico, 1971. Behavior of the electronic dielectric constant in covalent and ionic materials. Phys. Rev. B., 3: 1338-1350.

Singh, R.N., A.K. George and S. Arafin, 2006. Specific heat ratio, Gruneisen parameter and Debye temperature of crude oil. J. Phys. D: Appl. Phys., 39: 1220-1225.

Hecht, E., 2012. Optics, 1st Edn., Pearson Education India, ISBN-10: 8131718077, pp: 650.

Kang, E.S., J.Y. Bae and B.S. Bae, 2003. Measurement of thermo-optic coefficients in Sol-Gel Hybrid glass films. J. Sol. Gel Sci. Technol., 26: 981-984.

Abdellaoui, A., L. Martin and A. Donnadieu, 1988. Structure and optical properties of MoO_3 thin films prepared by chemical vapour deposition. Phys. Stat. Sol., 109: 455-462.

Miyate, N. and S. Akiyoshi, 1985. Preparation and electrochromic properties of rf-sputtered molybdenum oxide Films. J. Appl. Phys., 58: 1651-1655.

Rabalais, J.W., R.J. Colton and A. M. Guzman, 1974. Trapped electron in substoichiometric MoO_3 observed by X-ray electron spectroscopy. J. Chem. Phys. Lett., 29: 131-133.

Szekeres, A., T. Ivanova and K. Gesheva, 2002. Spectroscopic ellipsometry study of CVD molybdenum oxide films: Effect of temperature. J. Solid St. Electrochem., 7: 17-20.

Torres, J., J.E. Alfonso and L.D. Lopez-Carreno, 2005. XPS and X-ray diffraction characterization of MoO_3 thin films prepared by laser evaporation. Phys. Status Solidi C., 2: 3726-3729.

Pardo, A. and J. Torres, 2012. Substrate and annealing temperature effects on the crystallographic and optical properties of MoO_3 thin films prepared by laser assisted evaporation, Thin Solid Films, 520: 1709-1717.

Pergament, A.L., V.P. Malinenko, L.A. Aleshina, E.L. Kazakova and N.A. Kuldin, 2014. Electrical switching in thin film structures based on molybdenum oxides. J. Experimental Phys., 2014: 1-6.

Gehlig, R. and E. Salje, 1983. Dielectric properties and polaron conducting of WO_3 and $W_xMo1_{-x}O_3$. Phil. Mag. B., 47: 229-245.

Eagles, D.M., 1984. Optical absorption by mixed polaron.1. Theory. J. Phys. C: Solid State Phys., 17: 637-653.

Lakhno, V.D., 2013. Translation invariant theory of polaron (bipolaron) and the problem of quantizing near the classical solution. J. Experimental Theoretical Phys., 116: 892-896.

Dasgupta, B., Y. Ren, L.M. Wong, L. Kong and S.Y. Chiam *et al*., 2015. Detrimental effects of oxygen vacancies in electrochromic molybdenum oxides. J. Phys. Chem. C., 119: 10592-10601.

Peelaers, H., M.L. Chabinyc and C.G.V.D. Walle, 2017. Controlling n-type in MoO_3. J. Chem. Mater., 29: 2563-2567.

Mrowiecka, J.S., S.D. Diesbach, V. Maurice, S. Zanna and P. Marcus *et al*., 2008. Li-ion intercalation in thermal oxide thin films of MoO_3 as studied by XPS, RBS and NRA. J. Phys. Chem. C., 112: 11050-11058.

Anwar, M., C.A. Hogarth and K.A.K. Lott, 1989. ESR studies of thin films of MoO_3: Effects of substrate temperature, film thickness and annealing procedures. J. Mater. Sci., 24: 1660-1664.

Maruyama, T. and T. Kanagawa, 1995. Electrochromic properties of molybdenum trioxide thin films prepared by chemical vapour deposition. J. Electrochem. Soc., 142, 1644-1647.

Santhosh, S., M. Mathankumar, S.S.C. Sekaran, A.K.N. Kumar and B. Subramanian, 2017. Effect of ablation rate on the microstructure and electronic properties of pulsed- laser- deposited molybdenum oxide thin films, Lamgmuir, 33: 19-33.

Ritter, C., W. Muller-Warmuth and R. Schollhorn, 1985. Structure and motion of hydrogen in molybdenum bronzes H_xMoO_3 as studied by nuclear magnetic resonance. J. Chem. Phys., 83: 6130- 6138.

Devreese, J.T. and A.S. Alexandrov, 2009. Frohlichpolaron and bipolaron: Recent developments. Rep. Progr. Phys., 72: 066501.

Mott, N.F. and E.A. Davis, 1979. Electronic processes in non-crystalline materials. Oxford, Clarendon Press.

Arfaoui, A., S. Touihri, A. Mhamdi, A. Labidi and T. Manoubi, 2015. Structure, morphological, gas sensing and photocatalytic characterization of MoO_3 and WO_3thin films prepared by the thermal vacuum evaporation technique. Appl. Surf. Sci., 357: 1089-1096.

Tahini, H.A., X. Tan, S.N. Lou, J. Scott and S.C. Smith *et al*., 2016. Mobile polaronic states in α-MoO_3: An abinitio investigation of the role of oxygen vacancies and alkaline ions. ACS Appl. Mater. Interfaces, 8: 10911-10917.

Gesheva, K.A., T. Ivanova, G. Popkirov and F. Hamelmann, 2005. Optoelectronic properties of CVD MoO_3 and MoO_3- WO_3 films and their applications in electrochromic cells. J. Optoelecron. Adv. Mater., 7: 169-175.

Alexandrov, A.S. and J.T. Devreese, 2009. Advances in Polaron Physics. 1st Edn., Springer, Berlin, Germany, ISBN-10: 3642018963, pp: 167.